Title

Using Spectroscopy to Guide the Adaptation of Aptamers into Electrochemical Aptamer-Based Sensors.

Journal

Bioconjugate Chemistry, 34(1)

Authors

Wu, Yuyang
Ranallo, Simona
Del Grosso, Erica
et al.

Publication Date

2023-01-18

DOI

10.1021/acs.bioconjchem.2c00275

Peer reviewed

HHS Public Access

Author manuscript

Bioconjug Chem. Author manuscript; available in PMC 2024 January 21.

Published in final edited form as:

Bioconjug Chem. 2023 January 18; 34(1): 124–132. doi:10.1021/acs.bioconjchem.2c00275.

Using Spectroscopy to Guide the Adaptation of Aptamers into Electrochemical Aptamer-Based Sensors

Yuyang Wu,
Department of Chemistry and Biochemistry, University of California Santa Barbara, Santa Barbara, California 93106, United States

Simona Ranallo,
Department of Chemistry and Biochemistry, University of California Santa Barbara, Santa Barbara, California 93106, United States; Chemistry Department, University of Rome Tor Vergata, 00133 Rome, Italy

Erica Del Grosso,
Department of Chemistry and Biochemistry, University of California Santa Barbara, Santa Barbara, California 93106, United States; Chemistry Department, University of Rome Tor Vergata, 00133 Rome, Italy

Alejandro Chamoro-Garcia,
Department of Chemistry and Biochemistry, University of California Santa Barbara, Santa Barbara, California 93106, United States; Chemistry Department, University of Rome Tor Vergata, 00133 Rome, Italy

Herbert L. Ennis,
Department of Medicine, Columbia University, New York, New York 10032, United States

Nenad Milosavić,
Department of Medicine, Columbia University, New York, New York 10032, United States

Kyungae Yang,
Department of Medicine, Columbia University, New York, New York 10032, United States

Tod Kippin,
Department of Psychological and Brain Sciences, Department of Molecular Cellular and Developmental Biology, and Neuroscience Research Institute, University of California Santa Barbara, Santa Barbara, California 93106, United States

Francesco Ricci,
Chemistry Department, University of Rome Tor Vergata, 00133 Rome, Italy

Milan Stojanovic,

Corresponding Author: **Kevin W. Plaxco** – Department of Chemistry and Biochemistry, University of California Santa Barbara, Santa Barbara, California 93106, United States; Biological Engineering Graduate Program, University of California Santa Barbara, Santa Barbara, California 93106, United States; kwp@ucsb.edu.

The authors declare no competing financial interest.

Department of Medicine, Columbia University, New York, New York 10032, United States; Department of Biomedical Engineering and Systems Biology, Columbia University, New York, New York 10032, United States

Kevin W. Plaxco
Department of Chemistry and Biochemistry, University of California Santa Barbara, Santa Barbara, California 93106, United States; Biological Engineering Graduate Program, University of California, Santa Barbara, Santa Barbara, California 93106, United States

Abstract

Electrochemical aptamer-based (EAB) sensors utilize the binding-induced conformational change of an electrode-attached, redox-reporter-modified aptamer to transduce target recognition into an easily measurable electrochemical output. Because this signal transduction mechanism is single-step and rapidly reversible, EAB sensors support high-frequency, real-time molecular measurements, and because it recapitulates the reagentless, conformation-linked signaling seen in vivo among naturally occurring receptors, EAB sensors are selective enough to work in the complex, time-varying environments found in the living body. The fabrication of EAB sensors, however, requires that their target-recognizing aptamer be modified such that (1) it undergoes the necessary binding-induced conformational change and (2) that the thermodynamics of this “conformational switch” are tuned to ensure that they reflect an acceptable trade-off between affinity and signal gain. That is, even if an “as-selected” aptamer achieves useful affinity and specificity, it may fail when adapted to the EAB platform because it lacks the binding-induced conformational change required to support EAB signaling. In this paper we reveal the spectroscopy-guided approaches we use to modify aptamers such that they support the necessary binding-induced conformational change. Specifically, using newly reported aptamers, we demonstrate the systematic design of EAB sensors achieving clinically and physiologically relevant specificity, limits of detection, and dynamic range against the targets methotrexate and tryptophan.

Graphical Abstract

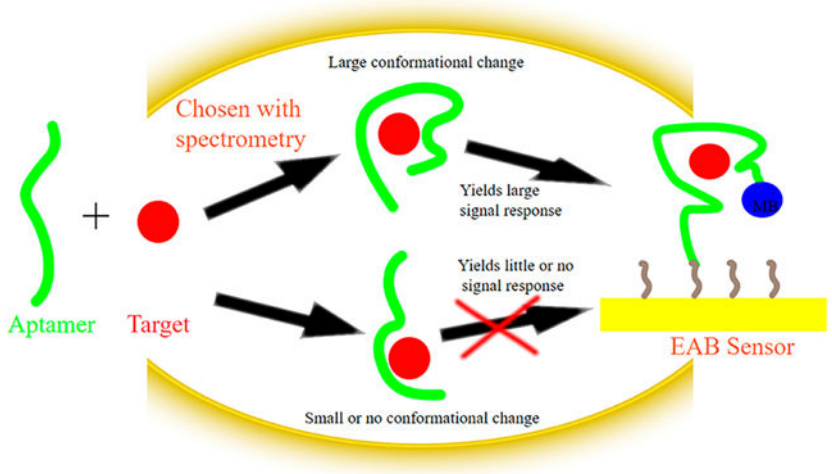

INTRODUCTION

Electrochemical aptamer-based (EAB) sensors are the only in vivo molecular sensing technology reported to date that is easily adaptable to new targets. That is, unlike the in vivo "continuous glucose monitor", which relies on the ability of glucose oxidase to convert its target into electrochemically detectable hydrogen peroxide,[1] signal generation in EAB sensors is linked to a binding-induced conformational change in its target-recognizing aptamer (Figure 1A), which is "read out" electrochemically (Figure 1B). Because this signal transduction mechanism is independent of the chemical reactivity of the targets, EAB sensors are highly versatile, and because it is reagentless, wash-free, and rapidly reversible, EAB sensors also support high-frequency, real-time molecular monitoring. Finally, because this transduction mechanism mimics the conformation-linked signaling seen in naturally occurring chemoperception systems, EAB sensors perform well when placed in the living body. Consistent with this EAB sensors have been used to perform seconds-resolved, real-time drug and metabolite concentration measurements in situ in the veins of live animals.[2–6] Indeed, the approach even supports closed-loop feedback control over plasma drug levels,[2,5] potentially ushering in an era in which drugs characterized by dangerously narrow therapeutic windows or highly complex, time-varying optimal plasma time courses can be delivered safely and effectively.

Although being independent of the reactivity of their targets greatly enhances the versatility of EAB sensors, expansion of the platform to new targets nevertheless still requires (1) the availability of an aptamer of appropriate affinity and specificity; and (2) its modification to introduce a large, binding-induced conformational change. In this paper, we demonstrate our approach to the latter issue. Specifically, while rational approaches to designing binding-induced conformational changes into aptamers have seen some success,[7–9] we most often achieve this goal via semiempirical destabilization of the aptamer through truncation or loop extension, such that the aptamer is predominantly unfolded at equilibrium.[10] Under such conditions, an aptamer still samples its folded state, and as, unlike the unfolded state, the folded state is competent to bind the target, target binding drives the folding equilibrium toward it, coupling target recognition to folding (Figure 1C). This "population shift mechanism" couples target recognition, however, to a thermodynamically unfavorable conformational change. This results in a trade-off: while further destabilization of the native state increases the number of molecules poised to respond to target, increasing gain, it also increases the unfavorable energy barrier that binding must overcome, reducing affinity.[11] We thus must "tune" the thermodynamics of the conformational switch (K_S, which is the equilibrium constant for the conformational change; see Figure 1C) for each new aptamer so as to achieve the optimal balance between these conflicting effects (between gain and affinity) for any given application.

We typically tune the conformational switching thermodynamics of our aptamers using empirical, spectroscopy-guided approaches. That is, although the modular nature of Watson–Crick base pairing renders it possible to predict the destabilizing effects of sequence variations on DNA secondary structure,[13] aptamer stability is often driven by non-Watson–Crick–Franklin tertiary interactions, the thermodynamics of which are far too poorly understood to enable their accurate prediction. Thus, while the modification of aptamers

to support binding-induced folding is generally easy, it usually requires several rounds of empirical trial-and-error. Here, we demonstrate our approach to this end, which employs fluorescent displacement assays and, when available, the intrinsic fluorescence of the target to monitor ligand binding, and circular dichroism to identify conformational states and binding-induced conformational changes.

RESULTS AND DISCUSSION

We started our work by selecting aptamers against the targets methotrexate, a commonly employed chemotherapeutic, and tryptophan, an essential amino acid. To generate high performance aptamers against these, we employed a solutionphase selection based on a stem-loop closing scheme.[14–16] In this, a constant region of the library hybridizes to an oligonucleotide attached to a column matrix. Any bindinginduced conformational change that disrupts this interaction (via, for example, stabilization of a stem formed from the library's complementary ends) frees the aptamer for elution and subsequent, additional rounds of amplification and enrichment (Figure 2A). Using an assay in which target binding displaces the dye thioflavin T from the binding site to produce a concomitant increase in fluorescence (Figure 2B), we determined that the parent (i.e., full-length, "as selected") methotrexate-recognizing aptamer binds its target with a dissociation constant of 6 ± 1 μM (all confidence intervals in this paper represent estimated 95% confidence levels) (Figure 2C). Likewise, the parent tryptophan-recognizing aptamer binds with a dissociation constant of 8 ± 2 μM. Both values fall below the clinically/physiologically relevant range for their respective targets, providing a "margin" to lose affinity during the process of adapting these aptamers into the EAB platform.

We first focused our aptamer modification efforts on our methotrexate-binding aptamer (Figure 3). We started this by modeling the aptamer's secondary structure using Nupack,[19] which, as expected for aptamers identified using our selection scheme, predicts that sequences near the 3′ and 5′ termini of the aptamer form a double-stranded stem with a short tail appended to the latter end (Figure 3A). We then generated a series of truncation constructs in which we shortened (first to 5 base pairs; "stem-5") and ultimately eliminated ("stem-0") the predicted double-stranded region. As our initial survey of these truncated variants, we used the intrinsic fluorescence of the methotrexate target to monitor the binding of the two longer constructs, stem-5 and stem-4, when unmodified and free in solution. That is, we titrated DNA sequences lacking either the surface-attaching thiol or the methylene blue redox reporter into a solution of methotrexate while monitoring the intrinsic fluorescence of the latter, which changes upon aptamer binding. From this we find that, while both constructs bind their target, the 1.0 ± 0.2 μM binding midpoint of stem-4 is about 2-fold poorer than the 0.55 ± 0.07 μM midpoint of the stem-5 construct (Figure 3B). This suggests that, because a higher target concentration is required to overcome the stem-4 construct's more unfavorable folding free energy, it is less stable than the stem-5 construct. Consistent with this, when we titrated methotrexate into solutions of these two constructs and monitored for conformational changes using circular dichroism spectroscopy, we observe that the stem-4 construct exhibits a larger change in ellipticity upon target binding (Figure 3C), suggesting that, in the absence of target, its unfolded state is more highly populated.

Guided by our initial, solution-phase spectroscopic studies, we next fabricated EAB sensors using the constructs stem-5, stem-4, stem-2, and stem-0. To interrogate these, we employed kinetic differential measurements[2] (KDM). This is a squarewave voltammetry approach in which we take the difference between signals collected at a higher square-wave frequency (80 Hz), at which the sensor responds to target with an increase in current, and a lower square-wave frequency (8 Hz), at which the sensor current is reduced by binding (Figure 1B). In addition to enhancing gain, KDM has provided an avenue to in vivo drift correction.[2–6] Using KDM to interrogate a sensor fabricated from our stem-0 construct, which entirely lacks the predicted double-stranded stem, we saw no significant change in EAB signal at any target concentration. This suggests that the stem-0 construct has either lost the methotrexate binding site or is so destabilized that it is not significantly refolded by even the highest methotrexate concentrations we employed (Figure 3D). Consistent with the latter hypothesis, the stem-2 construct achieves higher-gain, but this is associated with a rather high, 100 ± 15 μM binding midpoint, suggesting that the unfolded state of this aptamer is well populated in the absence of target (accounting for the high gain), but, conversely, the aptamer is so destabilized that it only begins to appreciably refold at quite high target concentrations. In contrast, the affinity of the stem-5 construct is better (binding midpoint 18 ± 7 μM), but its gain is poorer, suggesting that this construct is more stable than optimal. That is, that a large fraction of the aptamers are already folded in the absence of target, thus limiting the total signal change seen upon the addition of saturating target. Finally, under the conditions employed here the stem-4 construct represents a good tradeoff between gain (60%) and affinity (binding midpoint 27 ± 8 μM), producing a useful dynamic range nicely matching (Figure 3D) the plasma drug concentrations seen during highdose methotrexate treatment.[17]

While the useful dynamic range of the resulting EAB sensor matches clinical needs, the affinity of the stem-4 construct is about 30-fold poorer in the context of an EAB sensor than that of the unmodified aptamer when free in solution (Figure 3E). To elucidate the origins of this discrepancy we characterized the binding of a thiol-and-methylene-blue-modified stem-4 construct when free in solution using the intrinsic fluorescence of the methotrexate. While the synthesis cost of the modified aptamer precluded our going to high enough concentrations to map out the complete binding curve, it is clear that these modifications account for some, but not all, of the observed discrepancy. The remaining discrepancy presumably arises due to interactions between the aptamer and the self-assembled monolayer-coated surface of the gold electrode in the EAB sensor. Such interactions are known to destabilized folded DNA structures,[20] which would reduce affinity.

We next modified our tryptophan-binding aptamer (Figure 4A), the detailed selection of which will be described separately (Yang et al., under revision). As expected, given our selection scheme (Figure 2), this aptamer is also predicted to adapt a tailed stem loop structure. As our first effort we characterized a truncation variant of the aptamer, termed TRNC9/4. (As we explored constructs for this aptamer that went beyond stem deletion, we use a more cumbersome nomenclature for these: for this construct we removed 9 bases from the 5′ end, and 4 from the 3′ end). When free in solution, this construct exhibits a binding midpoint of 8 μM (Figure 4B, black curve) as determined using thioflavin T displacement assay, in which this fluorescent dye competes with the target for occupancy of

the target binding site. When we adapted this same construct into an EAB sensor, however, and interrogated it at a square-wave frequency of 200 Hz, the binding midpoint shifted to approximately 5 mM (Figure 4B). This latter value, which is more than 600-times higher than the midpoint we observed when we employ the dye displacement assay to monitor this same construct in solution, pushes the useful dynamic range of the resulting EAB sensor far too high to be of value in the monitoring of tryptophan, the physiological range of which is 20 to 100 μM in plasma.[18]

Detailed investigation of the binding curve of the EAB sensor suggested a possible origin to this enormous change in affinity. Specifically, whereas the EAB signals collected at this square-wave frequency (200 Hz) fit the single-binding site model somewhat poorly, they fit a two-site model quite well, producing dissociation constants of 4.3 ± 0.7 μM and 5.6 ± 0.2 mM (Figure 4B). This suggests that the discrepancy may be occurring because the aptamer presents two binding sites: a higher-affinity site that produces a thioflavin T signal but little EAB signal change at this square-wave frequency, and a loweraffinity site producing a large EAB signal change but little change in thioflavin T fluorescence. Additional evidence supporting this hypothesis is provided by the EAB sensor's square-wave frequency dependence. Specifically, at lower square-wave frequencies the higher-affinity binding event becomes quite apparent (Figure 4C). In contrast, at higher square-wave frequencies, the lower-affinity binding event dominates the signal (see Table S1 for details). We presume the lower-affinity binding site is fortuitous (was not selected for) and simply reflects the fact that the large, planar indole ring of tryptophan can bind somewhat nonspecifically to DNA once its concentration reaches many millimolar, a level orders of magnitude beyond physiological relevance.

The small EAB signal produced by the higher-affinity bind site suggests that the first construct we characterized may be fully folded in the absence of target. This in turn suggests that destabilization via further truncation could improve the EAB signal gain associated with binding to the high-affinity site. Thus motivated, we generated a series of truncation constructs (Figure 5A) that we first characterized using circular dichroism to monitor the urea-driven denaturation of the constructs to ascertain which might be unfolded in the absence of target (Figure 5B). Doing so we find that, as we suspected, the ellipticity of our longer constructs (TRNC9/4, TRNC15/9) changes significantly upon titration with urea, suggesting that they folded in the absence of target and then unfold as the concentration of the denaturant rises. Our shorter truncations (TRNC17/11 and shorter), in contrast, exhibit little change in ellipticity upon the addition of urea, suggesting they are unfolded in the absence of denaturant (and target). Building on this, we next used circular dichroism to check which of the latter constructs might refold in response to target binding. From this we found that the ellipticity of an intermediatelength truncation, TRNC17/11, increases significantly upon target addition until, at several millimolar tryptophan, it reaches a value similar to that seen for the (presumably already folded) TRNC9/4 construct (Figure 5C). In contrast, the more destabilized TRNC22/13 construct refolds only incompletely at the same high target concentration, and construct TRNC17/19 does not respond detectably to the target at any concentration.

Building on the results of our spectroscopic characterization, as our final study we converted the TRNC17/11 construct into a tryptophan-detecting EAB sensor. The resulting device achieves much greater gain than did our original, TRNC9/4 construct), with much of the increase in gain occurring at lower target concentrations. Thus, unlike its predecessor, the new sensor is well suited for monitoring physiological tryptophan levels in plasma (Figures 5D and S1).

CONCLUSIONS

Here we have used two newly selected aptamers to illustrate the manner in which we employ spectroscopic characterization to guide the design of novel EAB sensors. Specifically, we have demonstrated the use of fluorescence binding assays to monitor the solution-phase affinity of destabilized truncations, and circular dichroism and urea denaturation to monitor their possible conformational states and binding-induced conformational changes. While we concede that, given that our surveys were not exhaustive (did not characterize all possible truncations) and thus we might have missed still betterperforming constructs, by using these approaches we nevertheless rapidly generated EAB sensors achieving clinically or physiologically relevant limits of detection, dynamic ranges, and specificity for the measurement of the important targets methotrexate and tryptophan. The work presented here thus showcases the efficiency and success with which semiempirical, spectroscopy-guided aptamer modification can be used in the design new EAB sensors.

MATERIALS AND METHODS

Aptamer Selection.

All oligonucleotides used during selection were obtained from Integrated DNA Technologies (IDT; Coralville, IA, USA). Standard desalted oligonucleotides were used in selection, while testing in bimolecular format was done with modified oligonucleotides (e.g., fluorophore conjugates) that were HPLC purified by the manufacturer. All oligonucleotides were dissolved in nuclease-free water and stored −20 °C. All other materials and instruments were as detailed in our prior methods paper.[17]

The selections were carried out per previously published method,[17,18] except that here we used phosphate-buffered saline (PBS) as the standard selection buffer (Corning catalog number 21 0040 CV). The method is based on a structureswitching approach in which the target binding releases aptamer candidates from a library of oligonucleotides hybridized to a capture strand attached to a solid support (library and capture strand sequences are presented in Table 1). In the work described here, the polymerase chain reaction (PCR) amplifications we employed were run with first cycle at 95 °C for 2 min, N cycles at 95 °C for 15 s, 60 °C for 30 s, and 72 °C for 45 s, and last cycle at 72 °C for 2 min. The methotrexate (Alfa Aesar product, purchased though Thermo Fisher Scientific) and tryptophan (Sigma-Aldrich) were used as received.

For methotrexate we obtained the sequences from conventional cloning and read them through Sanger sequencing methods following the description in the referred literature.[17] The three sequences (Table 2) that were selected as aptamer candidates through Thioflavin T

dye displacement screening. Some bases (shown in parentheses in the table) were removed prior to the Thioflavin T dye displacement assay. The best performing of these (sequence MTX1) was moved forward for further characterization.

We optimized the Thioflavin T dye displacement assay used as our preliminary screen as in our previous study.[22,23] In brief, this used 400 nM oligonucleotide plus 4 μM Thioflavin T dye in PBS buffer, with varying concentrations of the targets. Each target concentration was tested in triplicate. Fluorescence measurements were performed with a plater reader (Molecular Devices Flexstation II) at room temperature with excitation and emission at 425 and 495 nm, respectively.

Aptamer Characterization.

Buffers and salts were obtained from Santa Cruz Biotechnology (Dallas, TX), methotrexate from Gold BioTechnology, Inc. (St. Louis, MO), and tryptophan from Thermal Fisher Scientific (Waltham, MA). All were used as received. Unmodified DNA sequences were used as received from IDT. The sequences employed are shown in Figures 4A and 5A.

We monitored the binding of the parent aptamers (Figure 2C) using the displacement of the dye thioflavin T. One volume of 1.6 μM aptamer solution was mixed with one volume of 16 μM dye and incubated for 40 min in the dark. Then one volume of 2× concentrated target solution was mixed with one volume of the dye/aptamer mixture to reach the desired final target concentration. After 40 min of incubation, we then measured the fluorescence (excitation at 425 nm, emission at 490 nm). We fit the resulting signal to the Langmuir isotherm to determine dissociation constants:

$$S(L) = S_0 + \frac{[L]\Delta S}{[L] + K_D} \quad (1)$$

where $S(L)$ is the signal seen in the presence of different concentrations of aptamer, S_0 is the background fluorescence seen in the absence of the ligand being added, $[L]$ is the ligand concentration, and ΔS is the difference in signal seen between the absence of ligand and saturating concentrations.

We characterized the affinities of the methotrexate-binding aptamer constructs (Figure 3B) in solution by adding increasing concentrations of the aptamer to PBS buffer (137 mM NaCl, 2.7 mM KCl, 10 mM Na_2HPO_4, and 1.8 mM KH_2PO_4) at pH 8.3 and containing 5 μM methotrexate. The fluorescence (excitation at 367 ± 10 nm, emission at 463 ± 10 nm) of each solution was measured after 15 min of equilibration and the resulting output fitted to the Langmuir isotherm to determine dissociation constants.

We also monitored the binding of stem-4 and stem-5 using circular dichroism (Figure 3C). To do so we prepared solutions of the constructs (2.5 μM for stem-5, 3.5 μM for stem-4) in PBS buffer at pH 7 in a 10 mm path length quartz cell and monitored their ellipticity as we added increasing concentrations of methotrexate, waiting 15 min after each addition. To determine for any background ellipticity of the cell and target we added increasing

concentrations of methotrexate to a PBS buffer solution without the aptamer. We then subtracted the ellipticity seen in this experiment from that determined during the titration of the aptamer.

We monitored the urea-induced unfolding of some truncation constructs of the tryptophan-binding aptamer (Figure 5B) as follows. We made solutions of 1 μM aptamer and the appropriate urea concentration in PBS buffer at pH 7.4 and containing 2 mM $MgCl_2$ and allowed them to equilibrate in a 1 cm path length cuvette for at least 3 min at 20 °C before then measuring their CD spectra on a J-1500 Circular Dichroism Spectrophotometer (Jasco Products Company, Oklahoma City, OK). We next used CD to monitor several of these constructs for possible binding-induced conformational changes (Figure 5C). To do so we first prepared 1 μM aptamer solution lacking tryptophan and 1 μM aptamer solutions containing 100 nM, 1 μM, or 10 μM tryptophan. We then mixed these to achieve each desired final tryptophan concentration. After equilibration for at least 3 min, we then recorded CD spectra.

Sensor Fabrication and Characterization.

Methyleneblue-and-thiol-modified aptamers were obtained from IDT and used as received. Carboxyl-modified methylene blue was added to the 3′ end of the constructs employed in EAB sensors via the formation of an amide bond to a primary amine on a 7-carbon linker, and a six-carbon thiol was attached to the 5′ end via a phosphoester bond. For example, the TRNC17/11 modified aptamer construct was: 5′-HO-(CH$_2$)$_6$-S-S-(CH$_2$)$_6$-O-PO$_2$O-CCGGTGGTGTAGTTCCGGCGTGGGGAAGG-CH_2-CH-(CH_2OH)-NH-C(O)-$(CH_2)_2$-MB-3′

We fabricated and characterized the methotrexate-detecting EAB sensors (Figure 3D) as follows. Briefly, we cut the 7.75 cm segments of gold wires (75 μm diameter, 64 μm insulation thickness, from A-M systems, Sequim, WA) and stripped their insulating coatings at both ends using a surgical blade. We insulated each wire with heat-shrinkable PTFE tubing (HS Sub-Lite-Wall, 0.02 in, black opaque from Zeus, Branchburg Township, CA) leaving on one end ~5 mm of exposed gold wire (working electrode). We left an exposed section on the other end of the wire that was long enough to allow electrical connections. Finally, we trimmed the exposed wire so the working electrode has a length of 3 mm. We then converted the gold surface into an E-AB sensor using the established protocol.[5,24] First, we performed an electrochemical cleaning using external reference and counter electrodes, immersing the gold working electrode into the cleaning solutions, (1) cycling the potential 300 times between −1 and −1.6 V (all potentials versus Ag/AgCl, from CH Instruments, Austin, TX) in a solution of 0.5 M NaOH at 1 V s^{-1} to remove any residual thiol/organic contaminants on the electrode surface; we rinsed electrode and performed (2) pulsing between 0 and 2 V for 16,000 cycles with a pulse length of 0.02 s in 0.5 M H_2SO_4 to increase the microscopic surface area in the electrodes (and thus signal current).[2] Because the manufacturer provides the DNA constructs in oxidized form, which does not effectively immobilize onto the gold surface, we must reduce the disulfide bond before deposition. To do so, we combined 2 μL of 10 mM Tris (2-carboxyethyl) phosphine (TCEP) per each μL of the DNA-aptamer at 100 μM, and incubated for a 1 h in the dark at room temperature. We

then adjusted the concentration of the reduced DNA to 500 nM based on its absorbance at 260 nm using 1× PBS. We immersed freshly cleaned gold electrodes in the aptamer solution for 1 h at room temperature, rinsed the electrodes with deionized water, and then incubated in 5 mM 6-mercapto-1-hexanethiol solution in 1× PBS overnight at 4 °C protected from the light. We rinsed the sensors with deionized water before using for measurements.

We fabricated and characterized tryptophan-detecting EAB sensors (Figures 4 and 5) as follows. We exposed 3 mm of gold wire (the rest being covered by polytetrafluoroethylene insulation) and cleaned these by cycling the potential at least 500 times between −1.0 V and −1.8 V (all potentials versus Ag/AgCl) at 2 V/s in 0.5 M NaOH. We then immersed them in 0.1 M H_2SO_4 and cycled the potential two times between 1.50 and −0.35 V at 100 mV/s. Following this we rinsed the freshly cleaned electrodes with deionized water before immersing them in 200 nM reduced DNA solution for 1 h. The latter was made by reducing the disulfide bond in the stock alkanethiol-modified, methylene-blue-modified DNA by combining 12 μL of 10 mM tris (2-carboxyethyl) phosphine with 2 μL of 100 μM DNA for 1 h in the dark, followed by dilution to 200 nM with PBS buffer. After DNA deposition, the electrodes were transferred to a 1 mM solution of 6-mercapto-1-hexanol in PBS and stored overnight until used. We rinsed the sensors with deionized water before using for measurements.

We performed electrochemical interrogation of all EAB sensors on a CHI 630E Electrochemical Workstation (CH Instruments, Austin, TX) using square-wave voltammetry (SWV) over the potential range −0.20 to −0.45 V. We used a standard three-electrode setup employing a platinum counter electrode and a Ag/AgCl (3 M KCl) reference electrode (CH Instruments). We employed a square-wave amplitude of 25 mV and the square-wave frequencies indicated below. All measurements were performed at room temperature and after at least 3 min equilibration.

To produce EAB binding curves (e.g., Figure 5C) we extracted square-wave voltammetric peak currents at each target concentration. We converted these into “normalized signal change” by determining the percentage difference between the peak current seen at a given target concentration to the corresponding peak height measured in a PBS blank:

$$\text{Normalized Signal (\%)} = \frac{I_{\text{target}} - I_{\text{Blank}}}{I_{\text{Blank}}} \times 100\% \tag{2}$$

Kinetic differential measurements (KDM) were calculated by taking the difference between the normalized signal seen at the lower frequency and that seen at the higher frequency. For the methotrexate sensor, these two frequencies are 8 and 80 Hz, and for the tryptophan sensor these are 15 and 200 Hz. We fit these data sets to the Langmuir isotherm to determine the dissociation constant of each construct. For the tryptophan construct TRNC9/4 we also fit the data to the sum of two Langmuir isotherms:

$$S(T) = \frac{[T]\Delta S_1}{[T] + K_{D1}} + \frac{[T]\Delta S_2}{[T] + K_{D2}}$$

(3)

where $S(T)$ is the EAB sensor KDM signal seen in the presence of different concentrations of target, $[T]$ is the target concentration, ΔS_1 and ΔS_2 are the changes in signal associated with the two binding events, and K_{D1} and K_{D2} are their dissociation constants.

Supplementary Material

Refer to Web version on PubMed Central for supplementary material.

ACKNOWLEDGMENTS

The authors wish to acknowledge Martin Kurnik, Philippe Dauphin Ducharme, and Andrea Idili for first pursuing the use of circular dichroism for guiding aptamer modifications. This work was supported by NIH grant EB022015, by the Marie Skłodowska-Curie grant agreement ("DNA-NANO-AB" project no. 843179 to SR), by the Marie Skłodowska-Curie grant agreement ("ENZYME-SWITCHES" project no. 896962 to EDG), by the Marie Skłodowska-Curie grant agreement ("SmartBioSense" project no. 799332 to ACG). ACG is supported by a Veronesi Foundation fellowship.

REFERENCES

(1). Vaddiraju S; Burgess DJ; Tomazos I; Jain FC; Papadimitrakopoulos F Technologies for continuous glucose monitoring: current problems and future promises. J. Diabetes Sci. Technol. 2010, 4 (6), 1540–1562. [PubMed: 21129353]

(2). Arroyo-Curras N; Somerson J; Vieira P; Ploense K; Kippin T; Plaxco KW Real-time measurement of small molecules in awake, ambulatory animals. Proc. Natl. Acad. Sci. U.S.A. 2017, 114, 645–650. [PubMed: 28069939]

(3). Dauphin-Ducharme P; Yan K; Arroyo-Curras N; Ploense K; Zhang Y; Gerson J; Kurnik M; Kippin TE; Stojanovic M; Plaxco KW Electrochemical aptamer-based sensors for improved therapeutic drug monitoring and high-precision, feedback-controlled drug delivery. ACS Sens. 2019, 4, 2832–2837. [PubMed: 31556293]

(4). Li H; Li S; Dai J; Li C; Zhu M; Li H; Lou X; Xia F; Plaxco KW High frequency, calibration-free molecular measurements in situ in the living body. Chem. Sci. 2019, 10, 10843–10848. [PubMed: 34040713]

(5). Idili A; Arroyo-Curras N; Ploense KL; Csordas A; Kuwahara M; Kippin TE; Plaxco KW Seconds-resolved pharmacokinetic measurements of the chemotherapeutic irinotecan in situ in the living body. Chem. Sci. 2019, 10, 8164–8170. [PubMed: 31673321]

(6). Idili A; Gerson J; Kippin T; Plaxco KW Seconds-resolved, in situ measurements of plasma phenylalanine disposition in living rats. Anal. Chem. 2021, 93, 4023–4032. [PubMed: 33594890]

(7). Xiao Y; Piorek BD; Plaxco KW; Heeger AJ A reagentless, signal-on design for electronic aptamer-based sensors via targetinduced strand displacement. J. Am. Chem. Soc. 2005, 127, 17990–17991. [PubMed: 16366535]

(8). Xiao Y; Qu X; Plaxco KW; Heeger AJ Label-free electrochemical detection of DNA in blood serum via target-induced resolution of an electrode-bound DNA pseudoknot. J. Am. Chem. Soc. 2007, 129, 11896–11897. [PubMed: 17850085]

(9). Yu Z-G; Sutlief AL; Lai RY Towards the development of a sensitive and selective electrochemical aptamer-based ampicillin sensor. Sens. Actuators 2018, 258, 722–729.

(10). White RJ; Rowe AA; Plaxco KW Re-engineering aptamers to support reagentless, self-reporting electrochemical sensors. Analyst 2010, 135, 589–594. [PubMed: 20174715]

(11). Vallée-Bélisle A; Ricci F; Plaxco KW Thermodynamic basis for the optimization of binding-induced biomolecular switches and structure-switching biosensors. Proc. Natl. Acad. Sci. U.S.A. 2009, 106, 13802–13807. [PubMed: 19666496]

(12). White RJ; Plaxco KW Exploiting binding-induced changes in probe flexibility for the optimization of electrochemical biosensors. Anal. Chem. 2010, 82, 73–76. [PubMed: 20000457]

(13). Zuker M Mfold web server for nucleic acid folding and hybridization prediction. Nucleic Acids Res. 2003, 31, 3406–3415. [PubMed: 12824337]

(14). Yang K-A; Barbu M; Halim M; Pallavi P; Kim B; Kolpashchikov DM; Pecic S; Taylor S; Worgall TS; Stojanovic MN Recognition and sensing of low-epitope targets via ternary complexes with oligonucleotides and synthetic receptors. Nat. Chem 2014, 6, 1003–1008. [PubMed: 25343606]

(15). Yang K-A; Pei R; Stojanovic MN In vitro selection and amplification protocols for isolation of aptameric sensors for small molecules. Methods 2016, 106, 58–65. [PubMed: 27155227]

(16). Nakatsuka N; Yang K-A; Abendroth JM; Cheung KM; Xu X; Yang H; Zhao C; Zhu B; Rim YS; Yang Y; Weiss PS; Stojanovic MN; Andrews AM Aptamer–field-effect transistors overcome Debye length limitations for small-molecule sensing. Science 2018, 362, 319–324. [PubMed: 30190311]

(17). Howard SC; McCormick J; Pui CH; Buddington RK; Harvey RD Preventing and managing toxicities of high-dose methotrexate. Oncologist 2016, 21, 1471–1482. [PubMed: 27496039]

(18). Ogawa S; Fujii T; Koga N; Hori H; Teraishi T; Hattori K; Noda T; Higuchi T; Motohashi N; Kunugi H Plasma Ltryptophan concentration in major depressive disorder: new data and meta-analysis. J. Clin. Psychiatry 2014, 75, e906–e915. [PubMed: 25295433]

(19). Zadeh JN; Steenberg CD; Bois JS; Wolfe BR; Pierce MB; Khan AR; Dirks RM; Pierce NA NUPACK: analysis and design of nucleic acid systems. J. Comput. Chem. 2011, 32, 170–173. [PubMed: 20645303]

(20). Watkins HM; Vallée-Bélisle A; Ricci F; Makarov DE; Plaxco KW Entropic and electrostatic effects on the folding free energy of a surface-attached biomolecule: an experimental and theoretical study. J. Am. Chem. Soc. 2012, 134, 2120–2126. [PubMed: 22239220]

(21). Downs AM; Gerson J; Leung KK; Honeywell KM; Kippin T; Plaxco KW Improved calibration of electrochemical aptamer-based sensors. Sci. Rep 2022, 12, 5535. [PubMed: 35365672]

(22). Renaud de la Faverie A; Guedin A; Bedrat A; Yatsunyk LA; Mergny J-L Thioflavin T as a fluorescence light-up probe for G4 formation,. Nucleic Acids Res. 2014, 42, No. e65.

(23). Nakatsuka N; Abendroth JM; Yang K-A; Andrews AM Divalent cation dependence enhances dopamine aptamer biosensing. ACS Appl. Mater. Interfaces 2021, 13, 9425–9435. [PubMed: 33410656]

(24). Arroyo-Currás N; Scida K; Ploense KL; Kippin TE; Plaxco KW High Surface Area Electrodes Generated via Electrochemical Roughening Improve the Signaling of Electrochemical Aptamer-Based Biosensors. Anal. Chem. 2017, 89 (22), 12185–12191. [PubMed: 29076341]

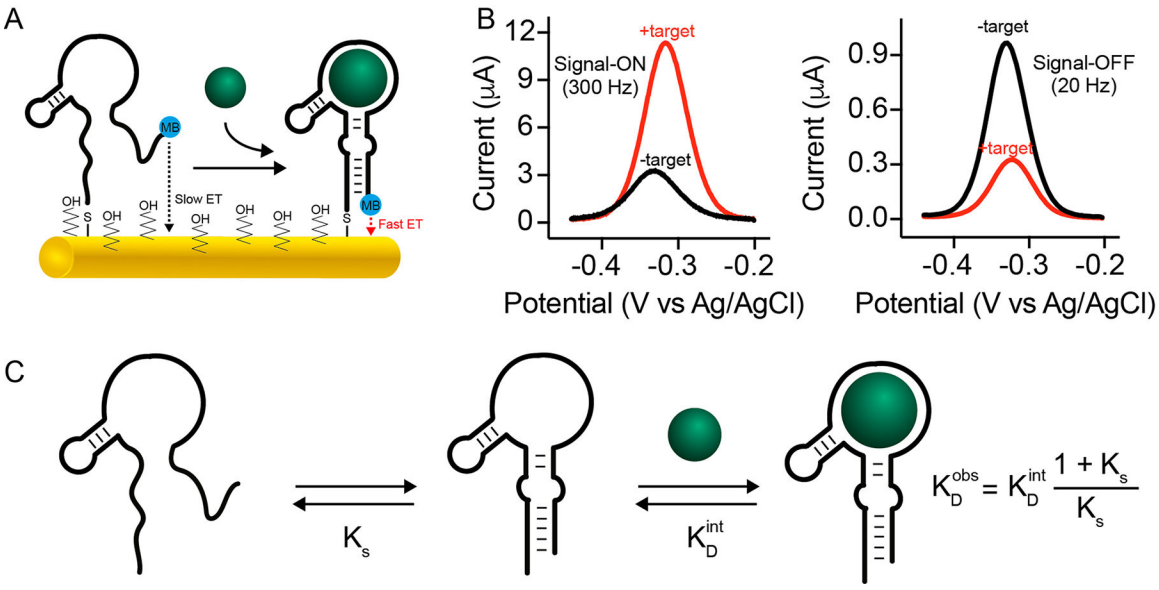

Figure 1.

(A) Signal generation in EAB sensors is driven by a binding-induced conformational change in its target-recognizing aptamer. This alters the efficiency with which an attached redox reporter (here methylene blue) transfers electrons to the sensor's electrode. (B) The resulting change in electron transfer rate is easily monitored using square-wave voltammetry, which can be tuned to increase ("signal on" behavior) or decrease ("signal off") its signal upon target binding by changing the square-wave frequency employed.[12] The data shown here are from our tryptophan sensor (TRNC17/11). (C) The population shift mechanism that EAB sensors employ entails a trade-off: pushing the conformational switching equilibrium toward the unfolded state increases gain (by increasing the number aptamers poised to respond to target) while simultaneously reducing affinity (by increasing the unfavorable folding free energy binding must overcome). Specifically, the observed affinity of the aptamer, K_D^{obs}, is a function of both the "intrinsic" affinity of the folded state, K_D^{int}, and the switching equilibrium constant, K_S.[11]

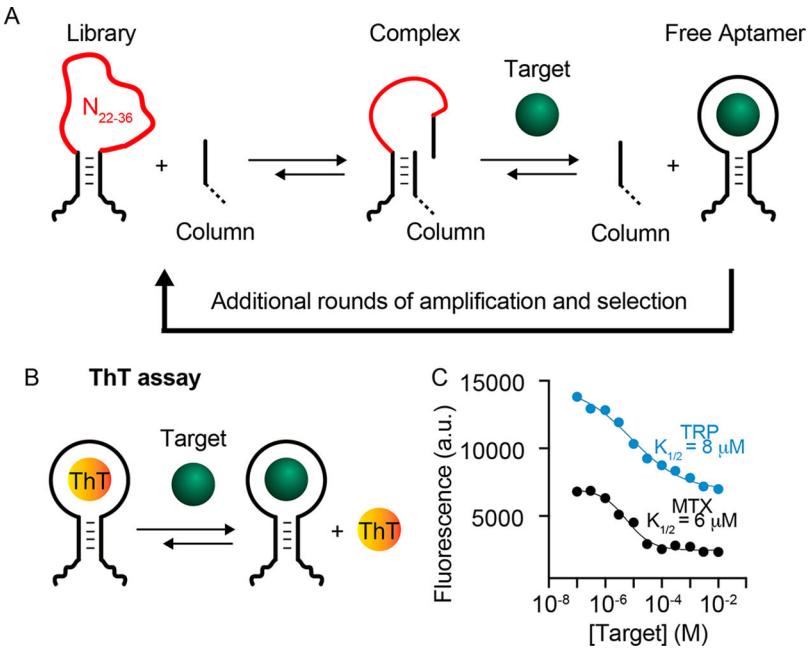

Figure 2.

(A) To generate the aptamers employed here we used a solution-phase selection based on a stem-loop closing scheme.[14–16] In this, a constant region of the library hybridizes to an oligonucleotide attached to a column matrix. Any binding-induced conformational change that disrupts this interaction (via, for example, stabilization of a stem formed from the library's complementary ends) frees the aptamer for elution and subsequent, additional rounds of amplification and enrichment. (B) For the preliminary characterization of the resulting aptamers we monitor the ability of the target to displace the fluorescent dye thioflavin T (ThT) from the aptamer's binding site. (C) The affinities of both of the aptamers described here match or exceed those needed for clinical applications. For example, plasma methotrexate levels (in high-dose methotrexate treatment)[17] are several hundred micromolar, and healthy plasma tryptophan levels[18] remain between 20 and 100 μM.

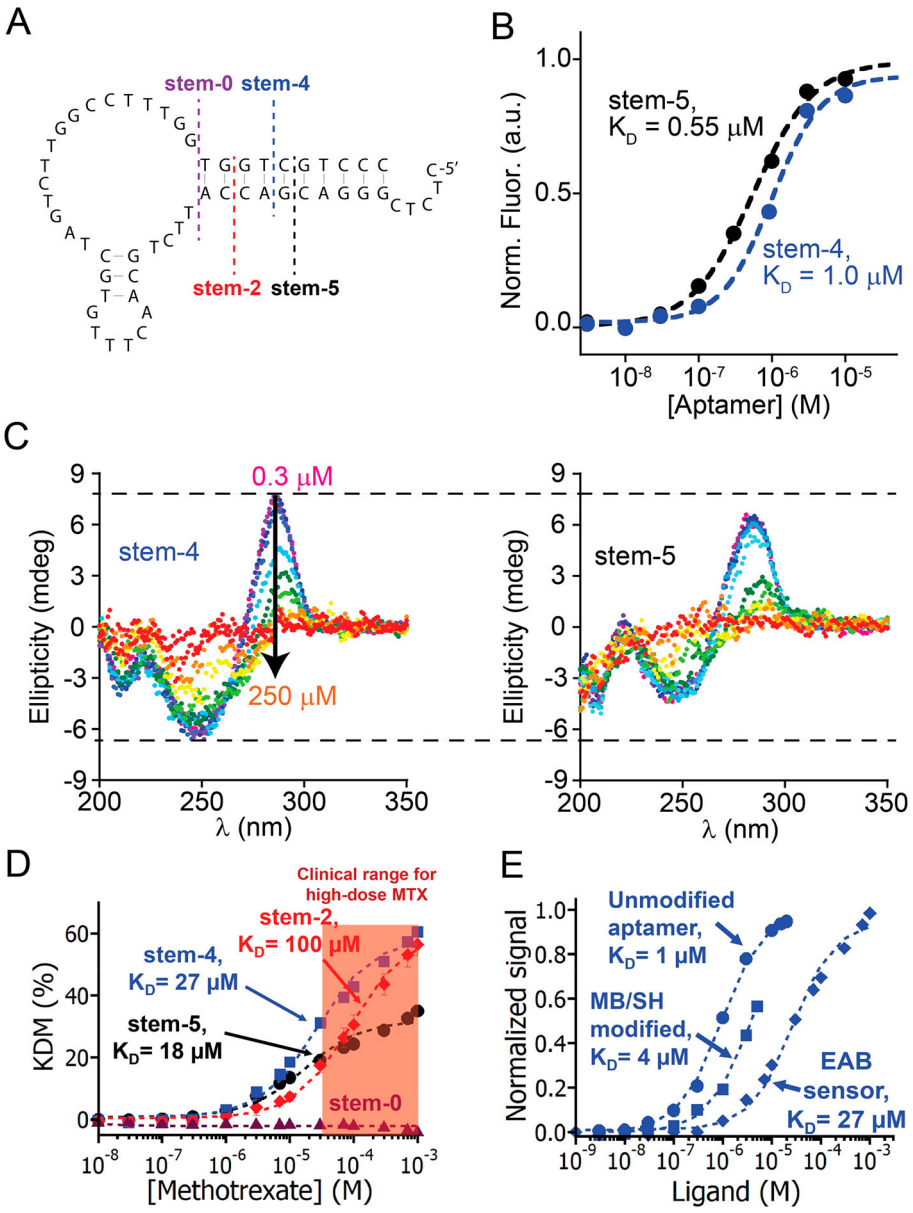

Figure 3.

(A) The methotrexate-binding aptamer is predicted to adopt a tailed stem-loop secondary structure, as expected given the nature of our selection scheme. Indicated are the four truncation variants that we have characterized here. (B) Using the intrinsic fluorescence of methotrexate to monitor the process, we first determined that the stem-5 and stem-4 constructs both bind their target with good affinity. (C) Circular dichroism studies of the binding of these same two constructs suggest that, while both undergo a significant conformational change upon target binding, the magnitude of the population shift may be greater for stem-4, suggesting it is, as expected, less stable. (D). Characterizing four constructs as EAB sensors (KDM = kinetic differential measurements, a square-wave voltammetry approach that enhances EAB signal gain[2]) we find that stem-4 reflects a good trade-off between affinity and signal gain, and produces a useful dynamic range that

nicely matches the plasma drug concentrations seen in high-dose methotrexate treatment.[17] (E) When incorporated into an EAB sensor, the affinity of stem-4 is significantly reduced relative to the affinity of the unmodified aptamer when free in solution. Characterization of the thiol-and-methylene-blue modified aptamer in solution indicates that some of this loss in affinity is due to the modifications required for EAB sensor fabrication, and some due to interactions with the electrode surface. Note, the K_Ds we have determined are likely approximate due to the limited upper baselines of our binding curves.

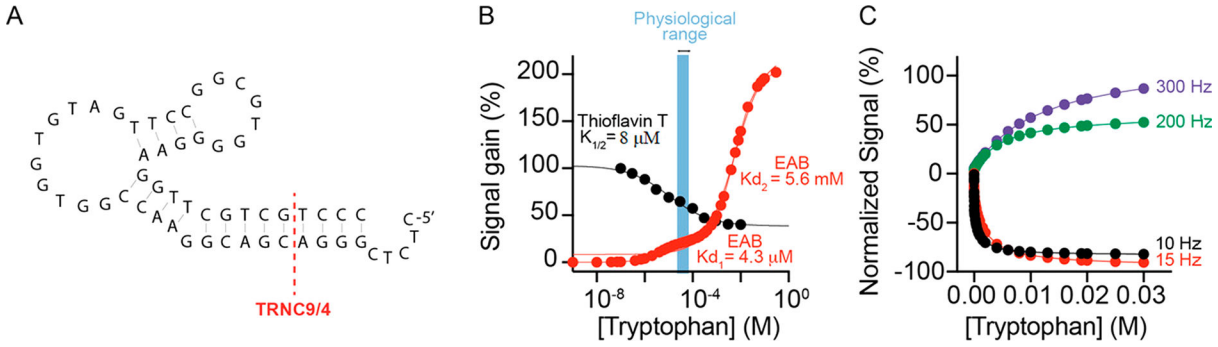

Figure 4.

When we adapt (A) the TRNC9/4 truncation of our tryptophan-binding aptamer into an EAB sensor its binding midpoint (B) moves to 700-fold higher concentrations than that seen when binding is monitored in solution using thioflavin T fluorescence. Noticing a small transition in the EAB binding curve at low target concentrations we hypothesized that this discrepancy occurs because the full-length aptamer binds two copies of its target, one at an affinity of ~1 μM and a second with affinity of several millimolar. Consistent with this, a two-site model fits the EAB data quite well (solid line; R^2 = 0.998), producing a small-amplitude event with a binding midpoint of 4.3 ± 0.7 μM and a much larger amplitude event with a binding midpoint to approximately 5 mM. Note: the EAB data shown here are reported as % change in KDM, with the KDM being derived from interrogations at square-wave frequencies of 15 and 300 Hz. (C) A study of the square-wave frequency dependence of the EAB sensor response curves provides further evidence in favor of this two-site hypothesis. Specifically, whereas the higher-affinity binding event is readily apparent at lower square-wave frequencies, at higher frequencies the lower-affinity binding event dominates the data (see Table S1 for the two-sitemodel fit parameters). Such strong frequency dependence to the binding curves is not typically seen for single-site aptamers.[21]

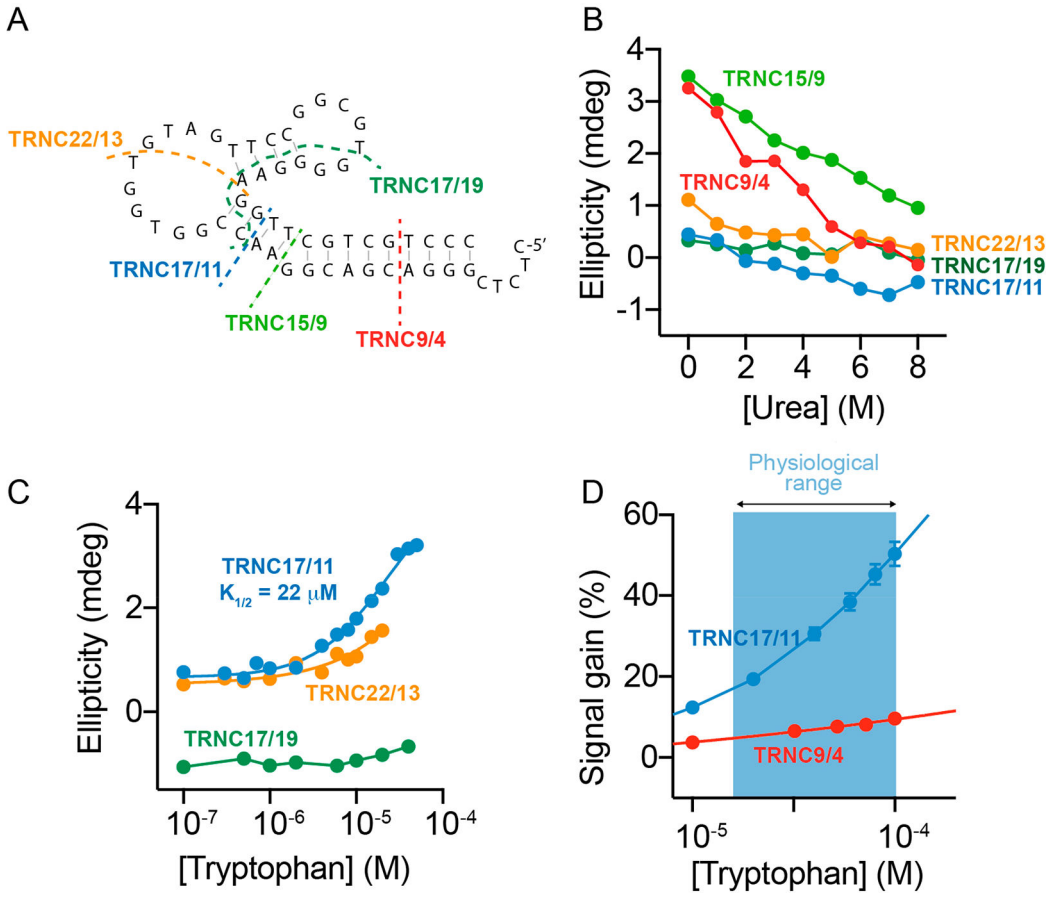

Figure 5.

(A) To modify the tryptophan-binding aptamer such that the high-affinity binding event produces a larger signal change we first characterized a series of truncations. (B) Performing "urea melts" on these (chemical denaturation) we find that, while the longer constructs (TRNC9/4, TRNC15/9) exhibit a significant change in ellipticity upon the addition of this denaturant, the shorter constructs do not, suggesting that the former are folded in the absence of denaturant and the latter unfolded. (C) Consistent with this, an intermediate length construct, TRNC17/11, undergoes a significant conformational change upon target binding. In contrast, the still more dramatic truncation, TRNC17/19, does not, presumably because it is so destabilized that that even the highest target concentrations used here are insufficient to overcome its conformational switching thermodynamics. (D) When employed in an EAB sensor, the intermediate truncation, TRNC17/11, produces significantly greater signal gain at clinical tryptophan levels (shown is the healthy plasma range) that does our original, TRNC9/4 construct. Note: the data shown here are reported as % change in KDM, with the KDM being derived from interrogation at square-wave frequencies of 300 and 15 Hz. (For the full binding curves, see Figure S1.)

Table 1.

Oligonucleotide Sequences Used in Our Selections

	Composition (5'→3')
N36 random library	GGA GGC TCT CGG GAC GAC-(N36)-GTC GTC CCG CCT TTA GGA TTT ACA G
Capture strand	5'-GTC GTC CCG AGA GCC ATA/3BioTEG/ *(biotinylated column immobilizing capture strand)*
Forward primer	GGA GGC TCT CGG GAC GAC
Reverse primer	CTG TAA ATC CTA AAG GCG GGA CGA C
Reverse primer (biotinylated)	/5Biosg/CTG TAA ATC CTA AAG GCG GGA CGA C

Table 2.

Methotrexate-Responsive Sequences

	Composition (5’ → 3’)[a]
MTX1	(ctctcgggac)gac CATTC TGCAA CTTTG TGCTA GTCTT GGCCT TTGGTG gtc(gtccc)
MTX2	(ctctcggg)acgac__---GGGACTT ATGGGCTGTT TGGGGGACCC ATATGAACG gtcgt(ccc)
MTX3	(ctctcggga)cgac CTTGGGA--- GAGGGATGTT TGGGGGGCCC CGTATAATG__gtcg(tccc)

[a]The small letters represent the conserved sequence elements in the library.